Eur. Phys. J. D **1**, 33–45 (1998)

THE EUROPEAN PHYSICAL JOURNAL D

Bright optical lattices in a longitudinal magnetic field. Experimental study of the oscillating and jumping regimes

C. Mennerat-Robilliard[a], L. Guidoni, K.I. Petsas[b], P. Verkerk, J.-Y. Courtois, and G. Grynberg

Laboratoire Kastler Brossel, Département de Physique de l'École Normale Supérieure, 24 rue Lhomond, 75231 Paris Cedex 05, France

Received: 9 October 1997 / Accepted: 6 November 1997

Abstract. All the bright optical lattices studied so far have been designed to obtain a circularly polarized light at the bottom of the optical potential wells. This condition minimizes the departure rate of the atoms from the fundamental adiabatic surface and permits an oscillating regime in a large range of parameters. We present here an experimental study of cesium atoms in a three-dimensional optical lattice, where the light is linearly polarized at the bottom of the potential wells. Temperature measurements and pump-probe spectroscopy give similar results for this lattice and for the conventional lin $\perp$ lin lattice (which have circular polarizations at the bottom of the wells) despite the fact that one lattice operates in the jumping regime and the other in the oscillating regime. We study the behaviour of the two types of lattices in a longitudinal magnetic field, with particular emphasis on the zero field and strong field regimes. The strong field situation is very simple because the eigenstates are then almost pure Zeeman substates and the adiabatic and diabatic potential surfaces are identical. The comparison between the zero-field and the high-field situations shows that the diabatic potentials are more appropriate to account for experimental observations in the novel lattice.

PACS. 32.80.Pj Optical cooling of atoms; trapping – 32.60.+i Zeeman and Stark effects

1 Introduction

Optical lattices [1] consist of cold atoms trapped in a periodic structure of potential wells induced by the interference of several laser beams. Although there have recently been a few studies on atomic propagation [2] and diffusion [3,4] inside such a lattice, most of the experiments done so far dealt with the localization and the oscillation [5–7] of atoms inside the optical potential wells. In these experiments, the light polarization at the bottom of the wells was *circular*. The origin of this choice of polarization can be traced back to the well-known one-dimensional (1D) model of sub-Doppler cooling [8] where the atoms interact with two linearly cross-polarized counterpropagating beams (lin $\perp$ lin configuration). Because of the light-shift of the ground state Zeeman sublevels, the lin $\perp$ lin configuration leads to the formation of a periodic structure of optical potential wells with light circularly polarized at the bottom of the wells. Further theoretical studies showed that the atoms are efficiently cooled and trapped inside the wells [9] and that the probability of escaping a well when the atoms are confined close to its bottom (Lamb-Dicke regime) is considerably reduced because of the circular polarization of light [10]. In fact, all the designs of bright optical lattices (*i.e.* optical lattices where the atoms are localized near points where their photon scattering rate is at a maximum) in one, two (2D) and three dimensions (3D) have matched this rule of circular polarization.

The first aim of this paper is to present a detailed investigation of an optical lattice where the light polarization is linear at the bottom of the wells [11]. In the following, we will refer to this lattice as Rot [lin $\perp$ lin] lattice because this lattice is obtained when the polarizations of the four beams of a 3D lin $\perp$ lin lattice are rotated by $\pi/2$. An experimental study performed with cesium atoms shows that this lattice has a cooling efficiency as good as the 3D lin $\perp$ lin four-beam optical lattice [12,13], and that the atomic localization inside the wells is also extremely good. The second goal of this paper is to present the behaviour of the two types of lattices in a longitudinal magnetic field. For small magnetic fields, a paramagnetic behaviour was shown in the case of the lin $\perp$ lin four-beam optical lattices [14]. A more detailed study was performed in the case of grey optical lattices operating on a $J \longrightarrow J$ or a $J \longrightarrow J-1$ transition [15]. In particular, it was shown that the dependence of the kinetic temperature of atoms in the grey lattices with the longitudinal magnetic field exhibits a sharp increase at low magnetic fields and a decrease at high magnetic fields. A similar dependence

[a] e-mail: robi@physique.ens.fr

[b] *Present address*: Instituto Nationale per la Fisica della Materia, Università degli Studi di Milano, Milano, Italy.

is found for the bright lattices operating on a $J \longrightarrow J+1$ transition. We also show that atomic localization is found in the two optical lattices studied here both at zero and high magnetic field. This situation of high magnetic field is particularly simple because the internal eigenstates are almost pure Zeeman sublevels. In the case of the lin $\perp$ lin four-beam lattice, one obtains a simple picture generalizing the initial theoretical models developed for $J = \frac{1}{2}$. Therefore this lattice also generally operates in the *oscillating regime*, *i.e.* the atoms undergo several oscillations in a well before leaving it. In the case of the Rot [lin $\perp$ lin] optical lattice, the transition rate between two Zeeman sublevels is *not* reduced by the atomic localization in the Lamb-Dicke regime. We have thus in this case an example of a lattice operating in the opposite regime, called *jumping regime*. Despite this apparently important theoretical difference, the experimental observations (temperature measurements, capture efficiency, probe transmission spectra) exhibit only very small differences. The third goal of this paper is to compare the use of the diabatic and adiabatic optical potentials for simple physical interpretations. In zero magnetic field the adiabatic and diabatic potential surfaces are different but they coincide in high field. The comparison between the data obtained in the zero and high magnetic field situations thus permits assessment of the relevance of these two potentials for a simple interpretation of the experimental results.

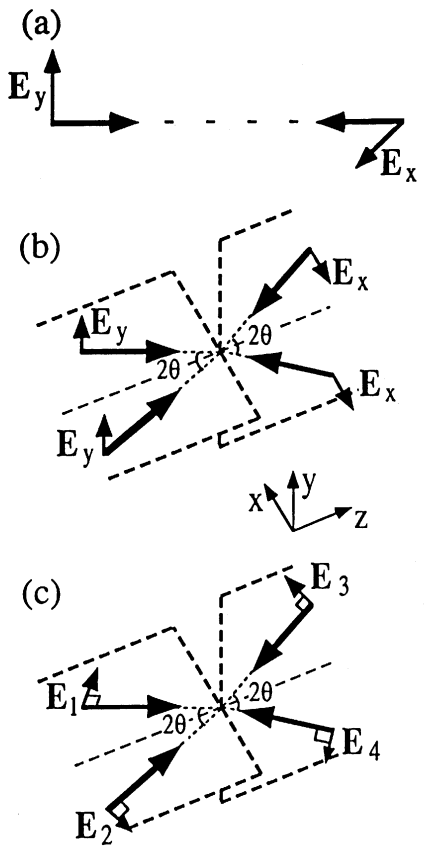

Fig. 1. a) The 1D lin $\perp$ lin configuration consists of two counterpropagating beams of the same frequency ω and crossed linear polarizations. b) Beam configuration in the 3D lin $\perp$ lin optical lattice. Two x-polarized beams propagate in the yOz plane and make an angle θ with the z axis. Two y-polarized beams propagate in the xOz plane and make the same angle θ with the z axis. c) Beam configuration for the Rot [lin $\perp$ lin] optical lattice. Two beams, linearly polarized in the yOz plane, propagate in this yOz plane, making an angle θ with the z axis. The two other beams, linearly polarized in the xOz plane, propagate in this xOz plane, making the same angle θ with the z axis.

2 3D generalizations of the 1D lin $\perp$ lin configuration

2.1 Electric fields

In the 1D lin $\perp$ lin configuration, two waves of frequency ω respectively polarized along the x and y axis counterpropagate along the z direction (Fig. 1a). As shown in [12], there are two simple methods for transforming this configuration into a four-beam configuration leading to a 3D optical lattice. The first method consists in splitting the x-polarized beam into two x-polarized beams making an angle 2θ that propagate in the yOz plane and the y-polarized beam into two y-polarized beams making an angle 2θ propagating in the xOz plane. This gives the lin $\perp$ lin four-beam lattice (Fig. 1b) that has been widely studied experimentally [2,4,7,13,14,16]. In the second method, the x-polarized beam is split into two beams respectively polarized along $\mathbf{e}_1 = \cos\theta\mathbf{e}_x + \sin\theta\mathbf{e}_z$ and $\mathbf{e}_2 = \cos\theta\mathbf{e}_x - \sin\theta\mathbf{e}_z$ that propagate in the xOz plane. The y-polarized beam is similarly split into two beams respectively polarized along $\mathbf{e}_3 = \cos\theta\mathbf{e}_y + \sin\theta\mathbf{e}_z$ and $\mathbf{e}_4 = \cos\theta\mathbf{e}_y - \sin\theta\mathbf{e}_z$ that propagate in the yOz plane (Fig. 1c) (the transition from one lattice to the other is performed through a $\pi/2$ rotation of all the polarizations, hence the name Rot [lin $\perp$ lin] given to the lattice shown in (Fig. 1c)). The main difference between the two light patterns is that the π-component is always equal to zero in the case of Figure 1b whereas a nonzero π-component can be found with the polarizations of Figure 1c. In fact, for small values of θ, the π-component remains small and the two lattices are expected to have similar properties. In both cases, the atoms are expected to be located in potential wells the bottom of which corresponds to circularly (σ^+ or σ^-) polarized light. However, when θ increases, the relative importance of the π-component also increases and the characteristics of the two lattices become more and more different. In particular, as shown in [12], the σ^+ and σ^- potential wells become unstable for the field configuration of Figure 1c when $\theta \geq 45°$. The atoms are then expected to be attracted into wells where the light has a polarization almost parallel to Oz. It is the first aim of this paper to study this uncommon situation.

We experimentally investigated two values of θ, one larger than 45° ($\theta \approx 55°$) and one below 45° ($\theta \approx 18°$). The field configuration of the Rot [lin $\perp$ lin] lattice leads

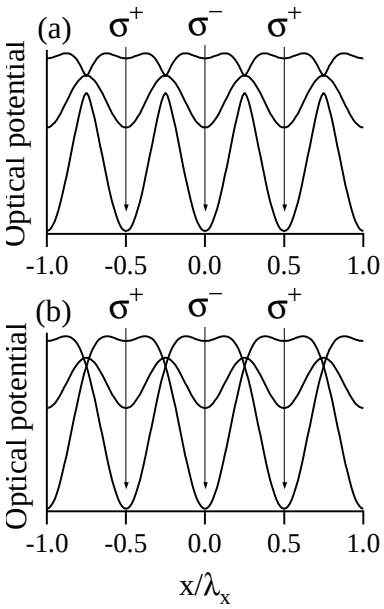

Fig. 2. Section of the (a) adiabatic and (b) diabatic potentials in the 3D lin ⊥ lin configuration along the $y = z = 0$ line for a $J_g = 1 \longrightarrow J_e = 2$ transition. The origin corresponds to a point of circular (σ^-) polarization of light.

to the following σ^+, σ^- and π components of the electric field:

$$\begin{aligned} E_{\pm}(\mathbf{r}) =& \sqrt{2}\cos\theta E_0 \left[\pm i \sin(k_s x)\exp(ik_c z)\right. \\ & \left. - \sin(k_s y)\exp(-ik_c z)\right] \\ E_{\pi}(\mathbf{r}) =& 2\sin\theta E_0 \left[\cos(k_s x)\exp(ik_c z)\right. \\ & \left. + \cos(k_s y)\exp(-ik_c z)\right] \end{aligned}$$

where E_0 is the amplitude of each lattice beam, $k_s = k\sin\theta$ and $k_c = k\cos\theta$. In the limit of small θ, E_π is small and the field configuration is not very different from the 3D lin ⊥ lin case. We thus expect similar physical observations for $\theta = 18°$ in the lin ⊥ lin and Rot [lin ⊥ lin] lattices. By contrast, for $\theta = 55°$, the π-component dominates the σ^+ and σ^- components and a clearly different physical situation is achieved.

2.2 Adiabatic optical potentials

The adiabatic optical potential is calculated by diagonalizing the reactive part of the atom-field coupling (light-shift) operator in the ground state Zeeman sublevels basis [17]. The adiabatic potentials for the 3D lin ⊥ lin lattice are well-known [1,12] and their shapes are qualitatively the same whatever θ (the only difference is a change of scale along the three spatial axis). We show in Figure 2a a section of the optical potential of such a lattice along the $y = 0$, $z = 0$ axis for a $J = 1 \longrightarrow J' = 2$ transition. The origin for this plot is taken at a point where the light is circularly σ^- polarized. The light polarization is always circular (σ^+ or σ^-) at the bottom of the wells.

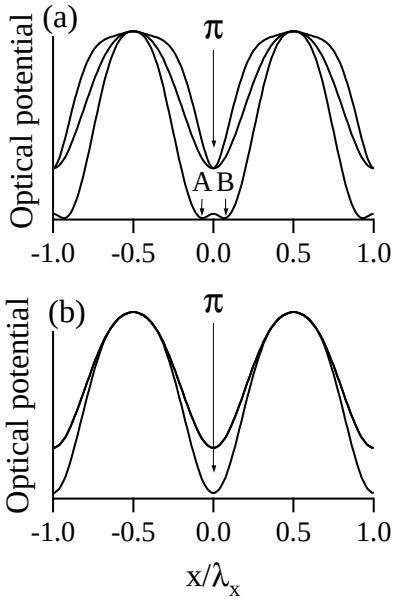

Fig. 3. Section of the (a) adiabatic and (b) diabatic potentials in the Rot [lin ⊥ lin] configuration with $\theta = 55°$ along the $y = z = 0$ line for a $J_g = 1 \longrightarrow J_e = 2$ transition. The origin is taken at a point where the light is linearly (π) polarized.

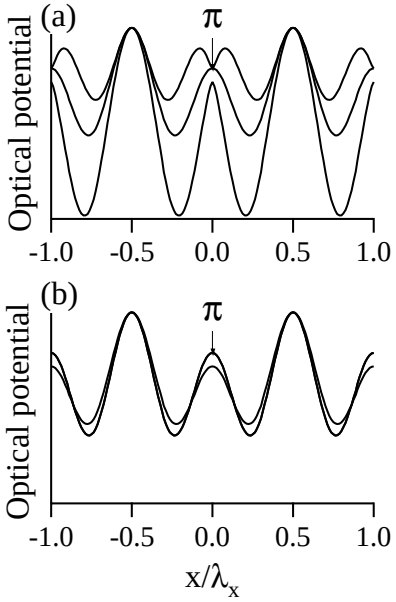

Fig. 4. Section of the (a) adiabatic and (b) diabatic potentials in the Rot [lin ⊥ lin] configuration with $\theta = 18°$ along the $y = z = 0$ line for a $J_g = 1 \longrightarrow J_e = 2$ transition. The origin is taken at a point where the light is linearly (π) polarized. Note that this section does not contain the absolute potential minima which are located in the $z = \pm\lambda/4$ planes, at points of circular polarization of light.

We now present the adiabatic potentials for the Rot [lin ⊥ lin] lattice The origin is taken at a point where the amplitude of the π-component of the electric field is maximum. The section of the adiabatic optical potential along the direction $y = 0$, $z = 0$ is shown in Figures 3a and 4a for $\theta = 55°$ and $\theta = 18°$ respectively. The lattice field

at the origin ($x = 0$) is π-polarized. In the case where $\theta = 55°$, two potential minima [A and B in Fig. 3a] are found. They correspond to points where the light polarization is elliptical but the z-component is dominant $\left(\frac{|E_\pi|}{|E_+|} = \frac{|E_\pi|}{|E_-|} \sim 9\right)$. It should also be noticed that the height U_h of the potential hill that separates the minima is much smaller than the depth U_0 of the optical potential well $\left(\frac{U_\mathrm{h}}{U_0} \sim 0.02\right)$.

In the case where $\theta = 18°$, no potential minimum is found in $x = 0$, $y = 0$, $z = 0$. The absolute minima of the adiabatic potential are found in the plane $z = \lambda_c/4$ (with $\lambda_c = 2\pi/k_c = \lambda/\cos\theta$) for $x = \frac{\pi}{2} + p\pi$, $y = \frac{\pi}{2} + p\pi$ (p integer). The light polarization at these points is circular. In fact, because E_π is small for $\theta = 18°$, the optical potential remains close to the potential of the 3D lin $\perp$ lin lattice.

2.3 Diabatic potentials

The diabatic potentials are obtained by keeping just the diagonal terms of the light-shift Hamiltonian in some reasonable basis. The difficulty is of course to define what "reasonable" means. In most cases, one relates the basis to the expected light polarization at the bottom of the wells. For example, in lin $\perp$ lin optical lattices, the light polarization is circularly polarized relative to an axis Oz. Hence the relevant basis is $|J, m\rangle$ where $m\hbar$ is an eigenvalue of $\hat{J}_z$. In the Rot [lin $\perp$ lin] lattice, the light polarization is linear parallel to Oz at the bottom of the wells for $\theta \geq 45°$ and we take the eigenstates of $\hat{J}_z$ as the relevant basis.

We show in Figure 2b the section of the diabatic potential along the $y = z = 0$ axis for the 3D lin $\perp$ lin lattice. The diabatic and adiabatic potentials nearly coincide close to the potential minima. Actually the only significant differences occur near the crossing points of the diabatic potential curves.

The diabatic potential curves for the Rot [lin $\perp$ lin] lattice along the $y = z = 0$ line are shown in Figures 3b and 4b for $\theta = 55°$ and $\theta = 18°$ respectively. The diabatic potential curves exhibit minima for $x = 0$ in Figure 3b (the lowest potential curve corresponding to $m = 0$). Note that the potential energy is the same for $m = \pm 1$, the upper curve is thus degenerate. By contrast, the same minima are not found for $\theta = 18°$. In this case, the absolute minima are located at points of circular polarization, as in the 3D lin $\perp$ lin lattice.

2.4 Adiabatic or diabatic potentials?

In principle, it is equivalent to use either potential as long as all terms are included in the Hamiltonian. However, the use of one type of potential is, in practice, often associated with some approximations. Basically, (*i*) the non-adiabatic motional couplings are often neglected when using the adiabatic potentials and (*ii*) the couplings originating from the non-diagonal elements of the light-shift operator are often neglected when one uses diabatic potentials. We wish now to give more insight into the range of validity of each of these approximations.

The adiabatic eigenstates $|j\rangle$ are generally space dependent. As a result, non-adiabatic couplings between different potential curves do exist. These couplings are of the order of $\langle l \left(\frac{\mathrm{d}}{\mathrm{d}t} |j(z(t))\rangle\right) = \langle l \left(\frac{\mathrm{d}}{\mathrm{d}z} |j\rangle\right) \frac{\mathrm{d}z}{\mathrm{d}t} \sim kv$ because the space variation of $|j\rangle$ occurs on a typical distance of the order of the wavelength λ. Non-adiabatic couplings are negligible if $kv \ll |E_i - E_j|$ where E_i and E_j are the adiabatic potentials. It thus appears that the adiabatic approximation is valid if the atoms do not reach the potential anticrossing (and crossing) points or if their velocity is relatively small close to these points. This approximation thus seems reasonable in the case of the lin $\perp$ lin lattice because the atoms are mostly located at the bottom of the wells (see Fig. 2a) far from the anticrossing points. By contrast, the approximation seems questionable in the case of the Rot [lin $\perp$ lin] lattice (Fig. 3b) for $\theta = 55°$ because the atoms cross the anticrossing points very often and with a very high speed, the anticrossing points being located near the minima of the potentials (in $x = 0$ for example). To have a more quantitative estimate of the validity of the adiabatic approximation in the Rot [lin $\perp$ lin] lattice, we can use $v \sim \sqrt{\frac{\hbar|\Delta'|}{M}}$ (where Δ' is an estimate of the light-shift and M is the atomic mass) to obtain $\hbar|\Delta'| \ll |E_i - E_j|^2 / E_\mathrm{R}$ (E_R is the recoil energy). In fact, near the potential minima, $E_i - E_j = D_{ij}|\hbar\Delta'|$ where D_{ij} roughly corresponds to a difference of squares of Clebsch-Gordan coefficients and the condition reads $\hbar|\Delta'| \gg E_\mathrm{R}/|D_{ij}|^2$. By using the numerical values of the Clebsch-Gordan coefficients, we find $\hbar|\Delta'| \gg 36E_\mathrm{R}$ for $J = 1 \longrightarrow J' = 2$ but $\hbar|\Delta'| \gg 2 \times 10^3 E_\mathrm{R}$ for $J = 4 \longrightarrow J' = 5$.

In the case where one uses diabatic potentials, one often neglects the non-diagonal terms of the light-shift operator in the investigation of the atom dynamics. If we denote by $|m\rangle$ and $|n\rangle$ diabatic states having diabatic energies E_m and E_n, and V_{mn} the non-diagonal part of the light-shift Hamiltonian, the validity range of the diabatic approximation is $|V_{mn}| \ll |E_m - E_n|$. This condition means first that the shape of the potentials is correctly described by the diabatic potentials and second that the transition probability from $|m\rangle$ to $|n\rangle$ during an optical pumping time Γ'^{-1} remains very small[1]. In the case of

[1] An order of magnitude of the transition probability is

$$P_{m\to n}\left(\Gamma'^{-1}\right) = \frac{|V_{mn}|^2}{|V_{mn}|^2 + (E_m - E_n)^2} \times \sin^2\left[\frac{\sqrt{|V_{mn}|^2 + (E_m - E_n)^2}}{\Gamma'}\right]. \quad (2.1)$$

If $|V_{mn}| \ll |E_m - E_n|$,
we find $P_{m\to n}\left(\Gamma'^{-1}\right) \ll 1$. (2.2)

the lin ⊥ lin lattice, the diabatic approximation fails near crossing points but, because the atoms do not reach these points very often, the diabatic approximation is a reasonable approximation for *localized* atoms. In the case of the Rot [lin ⊥ lin] lattice for $\theta > 45°$, one has $V_{mn} = 0$ at points where the light is π-polarized. At a distance a from these points $V_{mn} \simeq \hbar\Delta' C_{mn} ka$ (where C_{mn} is a number derived from Clebsch-Gordan coefficients). The diabatic approximation is thus valid for localized atoms, for which $C_{mn}ka \ll D_{mn}$. The range of values of a for which this condition is fulfilled is however narrow because $D_{01} < C_{01}$ (where $m = 0$ and $m = 1$ refer to Zeeman substates). The coupling due to V_{01} may thus be a limit to the validity of the diabatic approximation. In conclusion, the adiabatic and diabatic approximations can be applied to the lin ⊥ lin lattice although the former approximation is probably slightly more accurate. By contrast, for the Rot [lin ⊥ lin] lattice, none of the approximations looks obviously judicious. The comparison with the experimental data is thus essential to find out the best approximation.

2.5 Optical potential in a static longitudinal magnetic field

The addition of a static magnetic field B_0 along the direction z which is used to define the diabatic potentials is particularly useful to estimate the validity of the diabatic potential approximation. Indeed, for large values of B_0 (*i.e.* when the total Zeeman splitting $8\hbar g_{\rm F}\mu_{\rm B}B_0$, $g_{\rm F}$ being the Landé factor of the lower level and $\mu_{\rm B}$ the Bohr magneton, is much larger than the light-shift $\hbar|\Delta'|$) adiabatic and diabatic optical potentials coincide because the eigenstates then correspond to almost pure Zeeman substates. Furthermore the diabatic potentials for large B_0 coincide with the diabatic potentials for $B_0 = 0$ (apart from a non-essential translation of each potential curve due to the Zeeman effect). By comparing the data for $B_0 = 0$ and for large B_0, one can thus check the validity of the diabatic approximation and estimate the corrections originating from the non-diagonal elements of the light-shift operator.

The high magnetic field limit ($8\hbar g_{\rm F}\mu_{\rm B}B_0 \gg \hbar|\Delta'|$) corresponds to a simple physical situation analogous to the one encountered in the 1D lin ⊥ lin model for a $\frac{1}{2} \longrightarrow \frac{3}{2}$ transition. In particular, the lin ⊥ lin optical lattice in a large B_0 field is probably the simplest 3D generalization of this model, apart from the fact that the transfer of an atom from the $|F, m_{\rm F} = -F\rangle$ to the $|F, m_{\rm F} = F\rangle$ optical potential curve requires several optical pumping cycles[2]. In this case the atoms are expected to be trapped in potential wells associated with the $|F, m_{\rm F} = F\rangle$ substate near points where the lattice field is σ^+-polarized and in wells associated with $|F, m_{\rm F} = -F\rangle$ around points where the lattice field is σ^--polarized. The probability of escaping such a well by jumping into another potential surface is particularly low because of the small value (for large F) of the Clebsch-Gordan coefficient connecting $|F, m_{\rm F} = F\rangle$ and $|F' = F + 1, m_{\rm F'} = F - 1\rangle$.

[2] The cooling process does not necessarily require a passage from one extreme Zeeman sublevel to the other.

2.6 Oscillating and jumping regimes

The distinction between the oscillating and the jumping regimes of optical lattices was already presented in early laser cooling papers [9,17]. Basically, the jumping regime corresponds to a situation where the optical pumping is so fast that the atom remains in the same potential surface only for very short times. More precisely, an atom travels over distances much smaller than λ in the same potential well. As a result, the atom samples all the potential surfaces and the relevant force for the study of the atomic dynamics is an average force obtained by weighting the force in each surface by its occupation rate [17]. By contrast, in the oscillating regime, an atom remains for a long time in the same potential surface. In the case of lin ⊥ lin lattices, and more generally for all the lattices for which the light polarization is circular at the bottom of the wells, the usual regime is the oscillating regime. As shown in [10], this is because the optical pumping is much reduced by the strong localization of atoms (Lamb-Dicke limit) around points where the light is circularly polarized (an atom absorbing a σ^+ photon from the Zeeman substate $m = J$ can only return to the $m = J$ substate). By contrast, no such rule exists in the case of the other lattices and for example an atom in the potential wells of Figure 3b jumps from one potential surface to another with a rate of the order of Γ'. Because Γ' is generally much larger than the oscillation frequency, a Rot [lin ⊥ lin] lattice generally operates in the jumping regime when $\theta > 45°$.

This picture of the jumping lattice developed with the diabatic potentials of Figure 3b is certainly valid in the limit of large B_0 [11] where the diabatic and adiabatic potentials coincide. However, the relevance of this picture for $B_0 = 0$ might be questioned because one could argue using Figure 3a that the atoms are localized near the adiabatic potential minima, *i.e.* at points of elliptical polarization (with a dominant π-component). As shown in the following, comparison between the experimental data for small and large values of B_0 proves that the same regime is found in the two situations.

3 Kinetic temperature

We first compare the cooling efficiencies of the different lattices by measuring the kinetic temperature of the cesium atoms trapped in these lattices.

3.1 Experimental set-up

Cesium atoms are first cooled and trapped in a MOT, then the magnetic field and the laser beams of the MOT are switched off and the four lattice beams are switched on. These beams are tuned to the red side of the

$6S_{1/2}\,(F=4) \longrightarrow 6P_{3/2}\,(F'=5)$ transition, the detuning $\Delta = \omega - \omega_0$ from the atomic resonance varying between -6Γ and -30Γ (where Γ is the natural width of the excited state). The intensity I of the lattice beams can reach 40 mW/cm^2. In the case of the experiments performed in a longitudinal magnetic field, the procedure is the following. We first switch on the four lattice beams and when the atoms are thermalized in the potential wells, we establish the field B_0 in less than 1 ms. After 10 ms, we switch off both the lattice beams and the magnetic field and measure the kinetic temperature T_k of the cesium atoms along the Oy direction using a ballistic method (time-of-flight measurement). The probe beam for this measurement is located 10 cm below the position of the lattice[3]. In temperature measurements the scale for the horizontal axis is $\hbar\,|\Delta'|\,/E_R$ where Δ' is the total light-shift in the 3D lin $\perp$ lin lattice at a point where the light is circularly polarized and for a transition having a Clebsch-Gordan coefficient equal to 1[4]. We now give the results of temperature measurements for $B_0 = 0$ and for a large field[5]. The measurements made in the intermediate field regime are described in the Appendix A.

3.2 3D lin $\perp$ lin lattices

We show in Figure 5 the variation of T_k *versus* $\hbar\,|\Delta'|\,/E_R$ for the lin $\perp$ lin lattice with $\theta = 55°$ for $B_0 = 0$ (circles) and for $B_0 = 10$ G (squares). The total Zeeman splitting $8\hbar g_F \mu_B B_0$ is equal to 14000 E_R, which is a situation that corresponds to the high field limit (see Appendix A)[6]. The corresponding measurements for $\theta = 18°$ are shown in Figure 6. All these curves exhibit a linear variation for large values of Δ'/E_R. The values of the asymptotic slopes are given in Table 1. In particular, we remark that the slopes for $B_0 = 0$ are consistent with the value 24 nK/E_R measured by Gatzke *et al.* [16] for $\theta = 45°$.

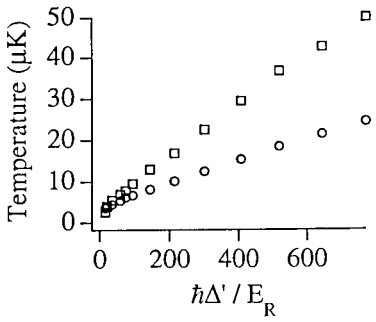

Fig. 5. Kinetic temperature measured by a time-of-flight method in the 3D lin $\perp$ lin lattice with $\theta = 55°$, in the case of $B_0 = 0$ (circles) and $B_0 = 10$ G (squares). The detuning is $\Delta = -30\Gamma$.

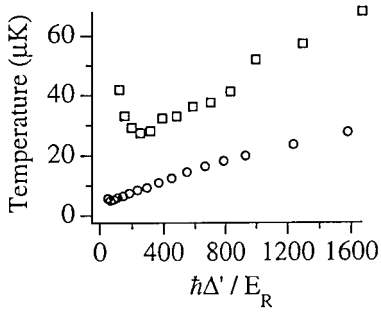

Fig. 6. Kinetic temperature measured by a time-of-flight method in the 3D lin $\perp$ lin lattice with $\theta = 18°$, in the case of $B_0 = 0$ (circles) and $B_0 = 8$ G (squares). The detuning is $\Delta = -20\Gamma$.

We note in both figures and in Table 1 that there is a significant difference between the temperatures for $B_0 = 0$ and for large B_0, the temperature being larger in the high field limit[7]. This observation shows that the diabatic approximation is not appropriate for calculating the temperature in low fields in a lin $\perp$ lin lattice.

3.3 Rot [lin $\perp$ lin] lattices

Similar temperature measurements were performed in the Rot [lin $\perp$ lin] lattices. The variation of T_k *versus* $\hbar\,|\Delta'|\,/E_R$ is given in Figures 7 and 8 for $\theta = 55°$ and $\theta = 18°$. The experimental conditions for these measurements were the same as those of Figures 5 and 6. We find here also linear asymptotes whose slopes are given in Table 1. The comparison between the values obtained for $B_0 = 0$ (circles) and large B_0 (squares) shows that the temperatures are very close for $\theta = 55°$ whereas a significant difference is found for $\theta = 18°$. The diabatic approximation thus seems to be reasonable for $\theta = 55°$. We also remark by comparing Figures 5 and 7 on the one hand and Figures 6 and 8 on the other hand that the

[3] The initial size of the atomic cloud ($\sim$ 1 mm) and the thickness of the probe beam (0.5 mm) lead to a correction of the order of -1 μK. Nevertheless, near the decrochage the effective size of the cloud is much smaller, leading to a correction that does not exceed -0.2 μK. We neglect this correction, which is always small compared to the measured temperature.

[4] The value of Δ' is deduced from the position of the transverse vibrational resonance of the lin $\perp$ lin lattice (see Sect. 5) without correction for the anharmonicity of the potential. Because of the difficulty to measure the lattice beams intensities precisely at the points where the atoms are located, we consider this method as more reliable, although the potential anharmonicity may lead to underestimate Δ' by a factor of the order of 20%.

[5] The temperatures we present here are slightly different from the ones published in [11,22]; we have indeed improved the technique of the measurements and the compensation of the earth magnetic field. Furthermore the temperature is not measured along the same direction.

[6] For such a large field, there is a significant difference ($\sim$ 5Γ) between the resonance frequency detuning Δ for $m = +4$ and $m = -4$. However the data were taken for detunings significantly larger than 5Γ ($\Delta = -20\Gamma$ for $\theta = 18°$ and $\Delta = -30\Gamma$ for $\theta = 55°$).

[7] Such a result is also found in 1D calculations using the band model (see Appendix A).

Table 1. Slope of the asymptotic linear variation of $k_{\rm B}T$ *versus* $\Delta'/E_{\rm R}$, in nK/$E_{\rm R}$. "Large B_0" means $B_0 = 8$ G for $\theta = 18°$ and $B_0 = 10$ G for $\theta = 55°$. Note that Δ' is deduced from the position of the vibrational resonance in a lin $\perp$ lin lattice without correction for the anharmonicity of the potential. Because the anharmonicity can be significant, this may lead to a possible systematic error.

	Lin $\perp$ lin, $\theta = 18°$	Lin $\perp$ lin, $\theta = 55°$	Rot [lin $\perp$ lin], $\theta = 18°$	Rot [lin $\perp$ lin], $\theta = 55°$
$B_0 = 0$	17 ± 1 nK/E_R	27 ± 1	13 ± 0.5	28 ± 1
Large B_0	30 ± 2	62 ± 2	23 ± 1	35 ± 1

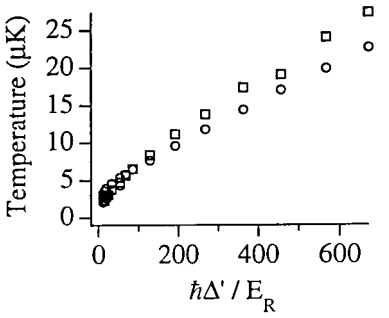

Fig. 7. Kinetic temperature measured by a time-of-flight method in the Rot [lin $\perp$ lin] lattice with $\theta = 55°$, in the case of $B_0 = 0$ (circles) and $B_0 = 10$ G (squares). The detuning is $\Delta = -30\Gamma$.

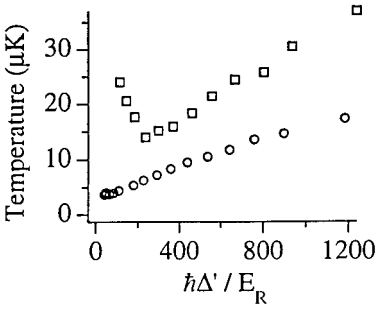

Fig. 8. Kinetic temperature measured by a time-of-flight method in the Rot [lin $\perp$ lin] lattice with $\theta = 18°$, in the case of $B_0 = 0$ (circles) and $B_0 = 8$ G (squares). The detuning is $\Delta = -20\Gamma$.

temperatures in the Rot [lin $\perp$ lin] lattices are equal to or smaller than the temperatures in the lin $\perp$ lin lattices. Optical pumping originating from the π component of the lattice field may thus assist the cooling process.

4 Atomic localization

4.1 Raman spectra

To study experimentally the localization of atoms in the lin $\perp$ lin and Rot [lin $\perp$ lin] optical lattices, we apply two probe beams, one along the z-axis (longitudinal probe) and one along the x direction (transverse probe). The two probe beams have the same intensity ($I_{\rm p} \simeq 0.1$ mW/cm^2) and the same frequency $\omega_{\rm p}$ which is scanned around the lattice frequency ω. We switch on one probe beam after the atoms are thermalized in the optical potential, and scan its frequency in 2 ms. This section is devoted to the presentation of results obtained when $\delta = \omega_{\rm p} - \omega$ is swept over a range of frequencies large enough that transitions between different potential surfaces can be observed. As shown in a previous work [18], these resonances are relatively broad because their widths are determined by the optical pumping rate. The narrower resonances associated with the vibrational motion which are found in the center of the spectrum, will be discussed in Section 5.

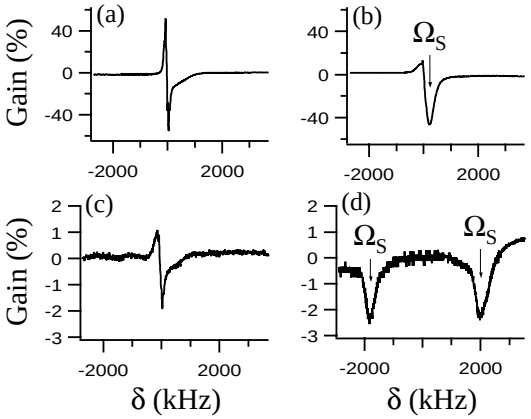

Fig. 9. Probe transmission spectra in the 3D lin $\perp$ lin lattice with $\theta = 55°$. The transverse probe is linearly polarized along Oy [(a) and (c)] and along Oz [(b) and (d)]. δ is the frequency detuning between the probe beam and the lattice beams. Spectra (a) and (b) correspond to $B_0 = 0$ while (c) and (d) correspond to $B_0 = 5$ G (*i.e.* a total Zeeman shift $8\hbar g_{\rm F}\mu_{\rm B}B_0 = 7000E_{\rm R}$). The detuning is $\Delta = -13\Gamma$ and the light-shift is $\hbar\Delta' = 550E_{\rm R}$. The resonances labelled $\Omega_{\rm S}$, observed only with a π-polarized probe, prove that the atoms are localized in σ^+ and σ^- sites.

4.2 3D lin $\perp$ lin lattices

We show in Figures 9 and 10, transverse probe transmission spectra in the lin $\perp$ lin lattices for $\theta = 55°$ and $\theta = 18°$. Each of these figures contains two curves obtained for $B_0 = 0$ with a probe polarization parallel to $\mathbf{e}_y$ (a) and to $\mathbf{e}_z$ (b), and two curves obtained for $B_0 = 5$ G for the same $\mathbf{e}_y$ (c) and $\mathbf{e}_z$ (d) probe polarizations. As expected from the fact that atoms are localized in potential wells where the light polarization is circular (σ^+ or σ^-), broad resonances labelled $\Omega_{\rm S}$ are observed for the π polarization of the probe. These resonances correspond to Raman transitions from $|F = 4, m = 4\rangle$ to $|F = 4, m = 3\rangle$ and from $|F = 4, m = -4\rangle$ to $|F = 4, m = -3\rangle$ (see Fig. 13a). Since

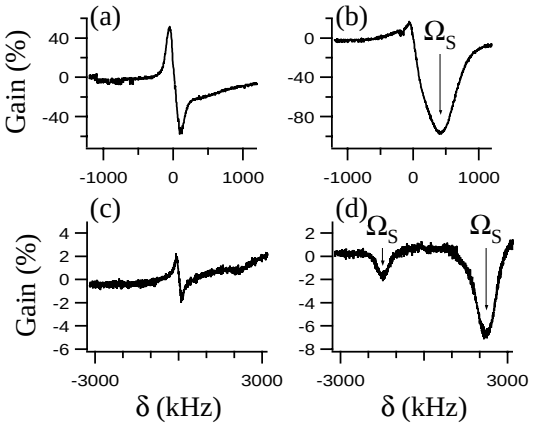

Fig. 10. Probe transmission spectra in the 3D lin ⊥ lin lattice with $\theta = 18°$. The transverse probe is linearly polarized along Oy [(a) and (c)] and along Oz [(b) and (d)]. δ is the frequency detuning between the probe beam and the lattice beams. Spectra (a) and (b) correspond to $B_0 = 0$ while (c) and (d) correspond to $B_0 = 5$ G. The detuning is $\Delta = -8\Gamma$ and the light-shift is $\hbar\Delta' = 1300E_R$. The resonances labelled Ω_S, observed only with a π-polarized probe, prove that the atoms are localized in σ^+ and σ^- sites. The fact that these resonances have different intensities in (d) is due to the fact that the scanning time of the probe frequency (2 ms) is on the same order as the lifetime of the lattice in large B_0 (5 ms).

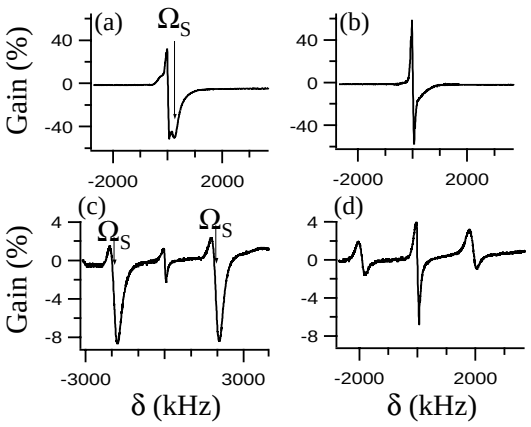

Fig. 11. Probe transmission spectra in the Rot [lin ⊥ lin] lattice with $\theta = 55°$. The transverse probe is linearly polarized along Oy [(a) and (c)] and along Oz [(b) and (d)]. δ is the frequency detuning between the probe beam and the lattice beams. Spectra (a) and (b) correspond to $B_0 = 0$ while (c) and (d) correspond to $B_0 = 5$ G. The detuning is $\Delta = -13\Gamma$ and the light-shift is $\hbar\Delta' = 500E_R$. The resonances labelled Ω_S, observed only with a σ-polarized probe (along Oy), prove that the atoms are localized in π sites.

the atoms are almost all in the $m = \pm 4$ Zeeman sublevels, the only Raman processes that can occur involve the absorption of a probe photon. That is why the Ω_S resonances exhibit essentially an absorption component, and hardly any amplification. In the case of the $\mathbf{e}_y$ polarization of the probe, a broad resonance associated with the $|F = 4, m = \pm 4\rangle$ to $|F = 4, m = \pm 2\rangle$ transition is expected but not observed because the Clebsch-Gordan coefficients lead to a much weaker intensity. The fact that these broad resonances are mainly observed with a π-polarized probe thus proves that the atoms are localized in σ^+ and σ^- sites. The difference in intensity in Figure 10d between the two Raman components is due to the fact that the scanning time of the probe frequency (2 ms) is of the same order as the lifetime of the lattice in large B_0 (~ 5 ms), so that the number of atoms trapped in the lattice is different at the beginning and at the end of the scan. We checked that the resonances have the same intensity by scanning the probe frequency in the other direction.

4.3 Rot [lin ⊥ lin] lattices.

We show in Figures 11 and 12 transverse probe transmission spectra in the Rot [lin ⊥ lin] lattices for $\theta = 55°$ and $\theta = 18°$. The subfigures follow the same order as in the previous Section: (a) and (b) correspond to $B_0 = 0$ and a probe polarization parallel to $\mathbf{e}_y$ (a) and $\mathbf{e}_z$ (b), (c) and (d) correspond to $B_0 = 5$ G and a probe polarization parallel to $\mathbf{e}_y$ (c) and $\mathbf{e}_z$ (d). It is immediatly evident that Figure 12 is almost identical to Figures 9 and 10. This shows that the same atomic localization is found in the Rot [lin ⊥ lin] lattice with $\theta = 18°$ and in the lin ⊥ lin lattices. Here again, the atoms are found in the lattice around points where the light is cicularly polarized.

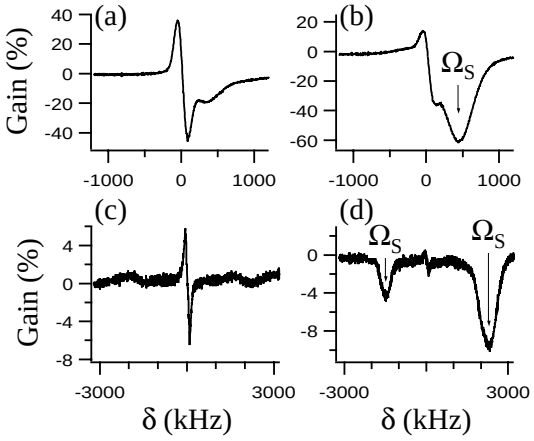

Fig. 12. Probe transmission spectra in the Rot [lin ⊥ lin] lattice with $\theta = 18°$. The transverse probe is linearly polarized along Oy [(a) and (c)] and along Oz [(b) and (d)]. δ is the frequency detuning between the probe beam and the lattice beams. Spectra (a) and (b) correspond to $B_0 = 0$ while (c) and (d) correspond to $B_0 = 5$ G. The detuning is $\Delta = -8\Gamma$ and the light-shift is $\hbar\Delta' = 1500E_R$. This figure is very similar to those concerning the 3D lin ⊥ lin lattices (Figs. 9 and 10). The resonances Ω_S are observed only with a π-polarized probe, which proves that the atoms are localized in σ^+ and σ^- sites. Resonances in (d) have different intensities because the scanning time of the probe frequency (2 ms) is on the same order as the lifetime of the lattice (5 ms for large B_0).

The spectra shown in Figure 11 are clearly very different. For $B_0 = 0$, the broad Ω_S resonance is observed with a $\mathbf{e}_y$-polarized probe (Fig. 11a) and is absent with the π-polarized probe (Fig. 11b). Such a result is consistent

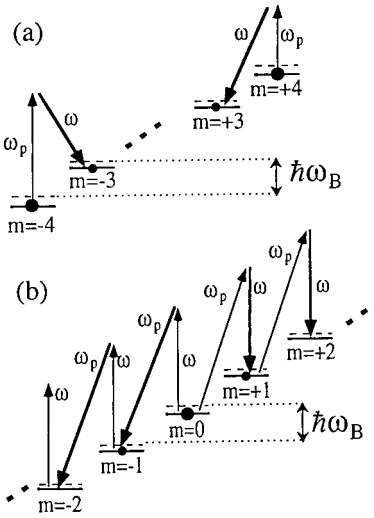

Fig. 13. Scheme of the Raman transitions that can occur between different potential surfaces in the large B_0 situation (a) in the 3D lin $\perp$ lin lattice and (b) in the Rot [lin $\perp$ lin] lattice. All the Zeeman sublevels are not shown. The circles representing the atomic populations in each level have no quantitative meaning. The dashed lines correspond to the Zeeman energy, and the bold lines represent the energy levels including both the Zeeman and the light shifts. ω is the lattice beams frequency while $\omega_{\rm P}$ is the probe beam frequency. In the case of the lin $\perp$ lin lattice, the main Raman transitions are obtained through the absorption of a photon in the π-polarized probe beam. In the case of the Rot [lin $\perp$ lin] lattice, Raman transitions with a probe polarized along Oy can induce amplification or absorption of the probe.

with the fact that atoms are localized close to points where the lattice field is linearly π-polarized. Atoms being in an eigenstate of F_z cannot undergo a Raman transition from a Zeeman sublevel m towards a different sublevel m' if both the probe and the lattice (pump) fields are π-polarized. By contrast, transitions from m to $m \pm 1$ can be induced by a π lattice field and the σ probe as shown in Figure 11a. The lineshape of these $\Omega_{\rm S}$ resonances is remarkably different from the one of the lin $\perp$ lin lattices. Figure 13b shows indeed that both an amplification and an absorption of the probe can occur, the atoms occupying almost all the Zeeman sublevels in a π-polarized light with relative occupation rates $\pi_0 = 0.34$, $\pi_{\pm 1} = 0.24$, $\pi_{\pm 2} = 0.08$, $\pi_{\pm 3} = 0.01$, $\pi_{\pm 4} = 0.0005$. Besides, the ratio of the amplitudes of the two components (amplification and absorption) is in good agreement with the ratio deduced from these occupation rates and Clebsch-Gordan coefficients. In the case where $B_0 = 5$ G, the situation is similar. Lateral resonances observed with the $\mathbf{e}_y$-polarized probe are clearly more intense than the resonances observed with the π-polarized probe, which is consistent with the fact that atoms are localized near points where the lattice field is nearly π-polarized. However the occurrence of the small lateral resonances in Figure 11d shows that the probability of finding atoms relatively far away from sites of pure π polarization is not negligible.

4.4 Fluorescence

It is also possible to obtain information about the atomic localization by measuring the relative absorptions for several probe polarizations or by measuring the different polarization components of the fluorescence emitted by the cesium atoms trapped in the lattice (without any probe beam). The former method was used in [11] but the interpretation of the results is not easy in the large B_0 limit because of the different Zeeman shifts experienced by the Zeeman sublevels. A narrow probe beam cannot be resonant on all transitions. To get a simple interpretation, we need large detunings and the signal-to-noise ratio becomes a serious problem. For this reason we present results obtained using the second method in this paper.

The experiments are realized with a frequency detuning $\Delta = -8\Gamma$ from resonance and a light shift $\hbar\Delta' = 600E_{\rm R}$ for $\theta = 55°$ and $\hbar\Delta' = 1400E_{\rm R}$ for $\theta = 18°$. Two values of the magnetic field, $B_0 = 0$ and $B_0 = 5$ G, are considered. We measured the $\mathbf{e}_y$ (σ) and $\mathbf{e}_z$ (π) fluorescence components along the Ox direction. The values of the ratio of the fluorescence intensities I_π/I_σ measured for the two lin $\perp$ lin lattices and the two Rot [lin $\perp$ lin] lattices are given in Table 2. We remark that the values found for the two lin $\perp$ lin lattices and the Rot [lin $\perp$ lin] lattice with $\theta = 18°$ are nearly the same and that similar values are found for $B_0 = 0$ and $B_0 = 5$ G. All these results are consistent with the same atomic localization in all these lattices. Furthermore, if all the atoms were localized exactly at the bottom of the wells, the atoms in $m_{\rm F} = +4$ would interact only with σ^+ light and those in $m_{\rm F} = -4$ with σ^- light, leading to a value $I_\pi/I_\sigma = 0$. The fact that the experimental values of I_π/I_σ are close to zero shows that the localization in these wells is very good. The values found for the Rot [lin $\perp$ lin] lattice with $\theta = 55°$ are markedly different. If all the atoms were exactly located at lattice points corresponding to a π polarization, we would expect from the steady-state values of the populations of the various $m_{\rm F}$ levels a ratio $I_\pi/I_\sigma \simeq 2.3$. The experimental results (see Tab. 2) are thus compatible with a confinement around points where the light is π-polarized, the confinement being better for $B_0 = 0$ than for $B_0 = 5$ G. Note that this latest observation also agrees fairly well with the Raman spectra of Figure 11. One possible, although probably partial, explanation for the looser confinement in large B_0 fields is that the temperature is slightly higher for the same value of the light shift (see Fig. 7).

5 Vibrational motion

5.1 3D lin $\perp$ lin lattice

The oscillation motion of atoms near the bottom of potential wells can be studied using probe transmission spectroscopy [1]. Raman transitions between different vibrational levels of the lowest potential wells are oberved as narrow sidebands located on each side of the Rayleigh line. The narrow width of these resonances was explained

Table 2. Fluorescence measurements obtained for $\Delta = -8\Gamma$ and $\hbar\Delta' = 600E_R$ for $\theta = 55°$ and $1400E_R$ for $\theta = 18°$. We give the ratio I_π/I_σ of the $\mathbf{e}_z$ (π) and $\mathbf{e}_y$ (σ) fluorescence intensities along the Ox direction.

	Lin $\perp$ lin, $\theta = 18°$	Lin $\perp$ lin, $\theta = 55°$	Rot [lin $\perp$ lin], $\theta = 18°$	Rot [lin $\perp$ lin], $\theta = 55°$
$B_0 = 0$	0.3 ± 0.1	0.2 ± 0.1	0.4 ± 0.1	1.9 ± 0.2
$B_0 = 5$ G	0.3 ± 0.2	0.3 ± 0.2	0.3 ± 0.1	1.5 ± 0.3

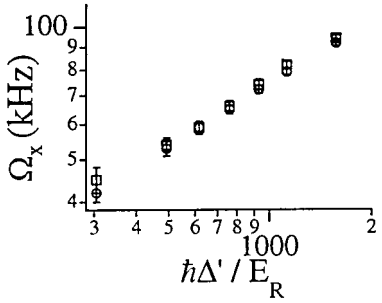

Fig. 14. Plot of the transverse vibrational frequency Ω_x in the 3D lin $\perp$ lin lattice with $\theta = 55°$ on a logarithmic scale, for a detuning $\Delta = -13\Gamma$. The circles represent the $B_0 = 0$ case whereas the squares correspond to $B_0 = 7$ G. The two curves are nearly superimposed. The slope for both curves is 0.48, in excellent agreement with the theoretical prediction of 0.5.

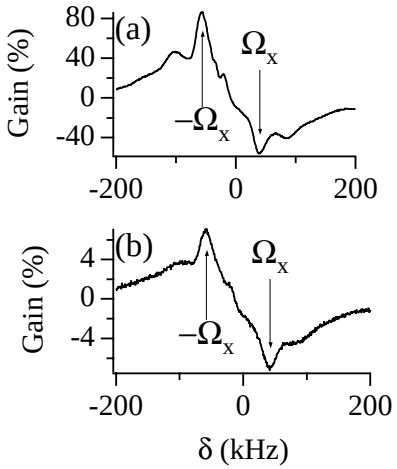

Fig. 15. Probe transmission spectra in the Rot [lin $\perp$ lin] lattice with $\theta = 55°$. The transverse probe is linearly polarized along Oz. $B_0 = 0$ (a) and $B_0 = 7$ G (b). δ is the frequency detuning between the probe beam and the lattice beams. The detuning is $\Delta = -13\Gamma$ and the light-shift is $\hbar\Delta' = 700E_R$. Apart from the amplitude of the resonances (*i.e.* the number of atoms trapped in the lattice), the spectra are almost identical.

as originating from the strong confinement of the atoms near points where the light is circularly polarized (Lamb-Dicke limit) [10]. We have repeated those experiments in the $\theta = 55°$ lattice to compare the vibrational frequencies for $B_0 = 0$ and $B_0 = 7$ G. We show in Figure 14 the position of the resonance Ω_x associated with the x vibrational motion *versus* $\hbar\Delta'/E_R$ on logarithmic axis[8]. The circles correspond to $B_0 = 0$ and the squares to $B_0 = 7$ G. In most circumstances, the circles and the squares are nearly superimposed. This shows that the curvature of the lowest potential curve is nearly the same for $B_0 = 0$ and $B_0 = 7$ G. Such a result is consistent with the fact that the diabatic potential (correct for large B_0) and the adiabatic potential have almost the same curvature for large values of the angular momentum F. Finally, we note that the slope of the line in Figure 14 is 0.48, in very good agreement with the value of 0.5 predicted by theory [1,16].

5.2 Rot [lin $\perp$ lin] lattice

The central part of the probe transmission spectra of Figure 11 also contains narrow vibrational peaks [11]. We discuss here the results obtained with a transverse probe and postpone to Appendix B the observations obtained with a longitudinal probe. We show in Figure 15a vibrational spectrum obtained for $B_0 = 0$ (a) and $B_0 = 7$ G (b) with a π-polarized transverse probe in the Rot [lin $\perp$ lin] lattice with $\theta = 55°$. The vibrational resonances Ω_x are located at almost the same position. This is illustrated by the plot of the position of the Ω_x resonances *versus* $\hbar\Delta'/E_R$ (Fig. 16)[4] for $B_0 = 0$ (circles) and $B_0 = 7$ G (squares). This observation proves that the dynamics is governed by very similar potentials for $B_0 = 0$ and $B_0 = 7$ G. Because the relevant potentials for large B_0 are the diabatic potentials, we may thus infer that the diabatic potentials are also appropriate for the situation in $B_0 = 0$. Finally we note that the slopes found in Figure 16 for $B_0 = 0$ and $B_0 = 7$ G are both equal to 0.41, in satisfactory agreement with the value 0.5 expected for a vibrational motion.

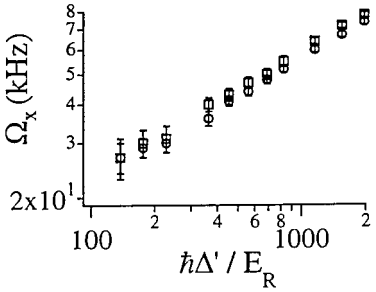

Fig. 16. Plot of the transverse vibration frequency Ω_x in the Rot [lin $\perp$ lin] lattice with $\theta = 55°$ on a logarithmic scale, for a detuning $\Delta = -13\Gamma$. The circles represent the $B_0 = 0$ case whereas the squares correspond to $B_0 = 7$ G. The slopes are 0.41 for both cases.

[8] The measurements are actually performed for a single value of Δ ($\Delta = -13\Gamma$) and the abscissa corresponds to the variation of the lattice beams intensity.

We remark however that the vibrational resonance in this Rot [lin ⊥ lin] lattice differs in nature from the resonances obtained in the lin ⊥ lin lattice. Because the atoms are localized near points where the light polarization is linear (π), about half of the scattering process induces a change in the potential surface. The time spent by an atom in a potential surface is thus on the order of Γ'^{-1} (contrary to the lin ⊥ lin case, there is here no Lamb-Dicke factor that lengthens this lifetime). As a result, most of the points obtained in Figure 16 correspond to the jumping regime of the lattice. The force that acts on the atom is an averaged force obtained by weighting the force experienced in each potential surface by its relative occupation probability. Because this averaged force attracts the atoms towards the bottom of the π potential wells with a strength proportional to the distance we recover an harmonic oscillation which gives rise to the vibrational sidebands of Figure 15. The averaged force being proportional to Δ', the vibration frequency varies as $\sqrt{\Delta'}$. The frequent jumps also help to reduce the width of the vibrational resonance because of a motional narrowing effect that prevents the inhomogeneous distribution of frequencies associated with each potential surface from being observed [11][9].

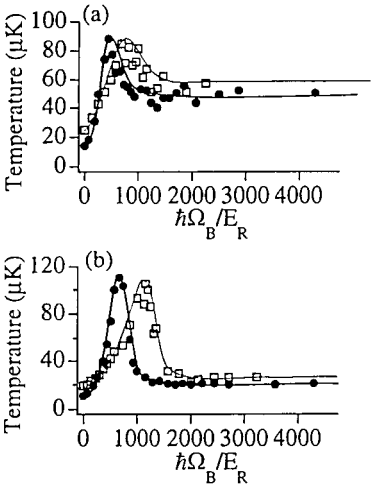

Fig. 17. Kinetic temperatures (measured by a ballistic method) as a function of the total Zeeman splitting $\hbar\Omega_{\rm B} = 8\hbar g_{\rm F}\mu_{\rm B}B_0$ created by the magnetic field B_0 in the 3D lin ⊥ lin (a) and the Rot [lin ⊥ lin] (b) lattices with $\theta = 55°$, for two values of the light-shift Δ'. The circles correspond to $\hbar\Delta' = 250E_{\rm R}$ whereas the squares correspond to $\hbar\Delta' = 600E_{\rm R}$. The detuning for these measurements was $\Delta = -10\Gamma$. The maximum of temperature is shifted to higher values of B_0 when the light-shift increases. Note that the lines are just to guide the eye and do not represent theoretical fits.

6 Conclusion

We have presented the results of an experiment in a 3D optical lattice where the light polarization is not circular at the bottom of the wells. Although the potential and the atomic dynamics (jumping instead of oscillating) are quite different from the lin ⊥ lin optical lattice, the temperature and the capture efficiency are quite similar. In fact, it appears that the cooling and capture efficiencies are quite robust because when we rotated in a random way the linear polarizations of the lattice beams, we always found atoms with a sub-Doppler temperature.

We also compared our experimental results with the predictions of adiabatic potentials (neglecting non-adiabatic transitions) and diabatic potentials (neglecting off-diagonal terms of the light-shift). In particular, we showed that many results in the Rot [lin ⊥ lin] lattice are more easily explained with the diabatic potentials when $\theta > 45°$. We also showed that the comparison between the data obtained in low and high magnetic fields hints at the importance of the terms neglected in the diabatic approximation. For example, it appears that these terms have a very small influence on the oscillation, the localization and the atomic temperature. On the other hand, we observed that atoms remain trapped for a longer time in the lattice when the magnetic field is zero (see Appendix A). The increase in the lifetime could be associated with the neglected terms. In fact, it seems that spatial diffusion remains one of the few important problems not yet fully understood in bright optical lattices. In the same spirit as the experiments presented in this paper, a quantitative comparison of the spatial diffusion in low and high fields could improve the understanding of this problem.

The authors are grateful to S. Guibal, C. Triché and W. Pokorski for stimulating discussions. This work was supported in part by the EU (TMR contract FRMX-CT96-0077). Laboratoire Kastler Brossel is an unité de recherche de l'Ecole Normale Supérieure et de l'Université Pierre et Marie Curie associée au CNRS.

Appendix A: Kinetic temperature versus magnetic field

We present in Figure 17 the variation of the kinetic temperature *versus* B_0 in the lin ⊥ lin (Fig. 17a) and in the Rot [lin ⊥ lin] (Fig. 17b) optical lattices[10] for $\theta = 55°$.

[9] We note finally that the same argument can be applied to the 1D experiment of Kozuma *et al.* [21].

[10] Whereas the velocity distribution can be nicely fitted by a Gaussian curve for $B_0 = 0$ and for $8\hbar g_{\rm F}\mu_{\rm B}B_0 \gg \hbar\Delta'$, this is no longer the case for intermediate fields. In particular, the velocity distribution exhibits extra peaks centered around $v \neq 0$. These peaks correspond to Raman transitions between different Zeeman sublevels [19] (see also C. Triché, Ph.D. thesis, Paris, 1997). The experimental temperatures reported in Figures 7 and 8 correspond to the width of the peak centered on $v = 0$. Note that the theoretical temperatures are associated with a determination of $\overline{v^2}$. This is a first reason why a quantitative agreement between experiment and theory is not expected. The other reasons are the different dimensionalities (3D and 1D) and transitions ($F = 4 \longrightarrow F' = 5$ and $F = 1 \longrightarrow F' = 2$).

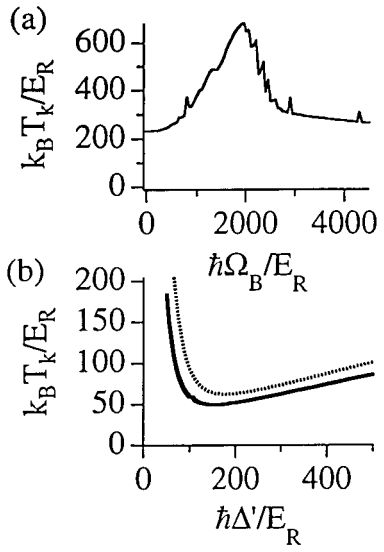

Fig. 18. Theoretical results obtained using the band model for a $F = 1 \longrightarrow F' = 2$ transition on the 1D lin $\perp$ lin configuration. (a) Variation of the kinetic temperature as a function of the total Zeeman splitting $\hbar\Omega_B$ created by a static magnetic field along Oz. The calculation was performed with a light-shift $\hbar\Delta' = 2000E_R$. The temperature is maximum when $\hbar\Omega_B \simeq \hbar\Delta'$. A few population resonances [20] are observed on the curve. (b) Evolution of the kinetic temperature as a function of $\hbar\Delta'$, in the case $B_0 = 0$ (solid line) and for a strong magnetic field, *i.e.* $\hbar\Omega_B \gg \hbar\Delta'$ (dashed line).

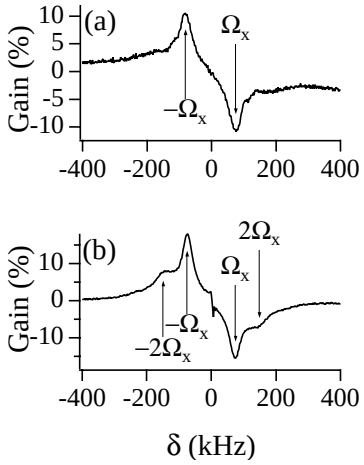

Fig. 19. Probe transmission spectra in the Rot [lin $\perp$ lin] lattice with $\theta = 55°$ (a) for a longitudinal probe (propagating in the z direction) linearly polarized along Ox and (b) for a transverse probe (propagating in the y direction) linearly polarized along Oz. δ is the frequency detuning between the probe beam and the lattice beams. The detuning is $\Delta = -6\Gamma$ and the light-shift $\hbar\Delta' \simeq 1600E_R$. The same fundamental vibrational resonance is observed on both spectra.

Such an experiment has been repeated for several values of the lattice beams intensity I and we show in Figure 17 the temperature dependence for two values of I. It can be seen that the position of the maximum is shifted to higher values of B_0 when I increases, a behaviour similar to the one found in grey lattices [15].

These observations are in agreement with our expectations. A 1D theoretical study of the atomic motion on the lin $\perp$ lin configuration, for a $F = 1 \longrightarrow F' = 2$ transition[11], using a full quantum treatment of the center of mass motion [9], shows that the kinetic temperature T_k increases with B_0 at low field, reaches a maximum when the total Zeeman splitting $\hbar\Omega_B = 2\hbar g_F \mu_B B_0$ is of the order of the light-shift $\hbar\Delta'$ (in agreement with the experimental observations) and decreases towards an asymptotic value when B_0 further increases (Fig. 18a) shows the theoretical variation of the temperature of the atoms as a function of Δ', when $B_0 = 0$ and in the strong field regime ($2\hbar g_F \mu_B B_0 \gg \hbar\Delta'$). The two curves exhibit similar variations but the temperature is slightly higher for large B_0 than for $B_0 = 0$, in agreement with the experimental observations (Figs. 5 and 6).

A striking difference between the zero field and the high magnetic field cases is the difference between the lifetimes of the lattices. Whereas the number of atoms in the lattice decreases with a time constant equal to 0.5 s for $B_0 = 0$ and $\theta = 55°$ (the same value is found for the lin $\perp$ lin and the Rot [lin $\perp$ lin] lattices), a much shorter value (5 ms for the lin $\perp$ lin lattice, 10 ms for the Rot [lin $\perp$ lin] lattice) is found for large B_0. We note that the cooling mechanism is remarkably simple in the high field limit because the adiabatic states coincide with the diabatic $|F, m_F\rangle$ substates and are thus independent of the position in the lattice. The non-diagonal terms in the light-shift Hamiltonian may help the trapping process[12].

Appendix B: Selection rules for the vibrational resonances in the Rot [lin $\perp$ lin] lattice

In the case of the lin $\perp$ lin lattice, a longitudinal probe only excites the Oz vibration motion [2]. This is however not a general rule and we show now that in the Rot [lin $\perp$ lin] lattice (with $\theta = 55°$), both a longitudinal and a transverse probe trigger the oscillation of a transverse mode. Such an unexpected result is first observed experimentally as shown in Figure 19 where we present a spectrum obtained with a longitudinal (a) and a transverse probe (b). The same vibration resonance is found[13]. This result holds whatever I and Δ.

We now show how this result can be explained from the expression of the operator that connects the initial and final states of the Raman transition. A Raman process

[11] The temperature dependence is similar for other transitions, but when $F > 1$ the variation of T is complicated by the occurrence of many population resonances (obtained in the secular regime [20]). We thus chose to present here the simplest case.

[12] Moreover one cannot exclude the fact that the bunching of velocities around a nonzero value as mentioned in footnote 10, although less important than for intermediate B_0, also contributes to the escape of atoms.

[13] The harmonics are different however.

consists of the absorption of a photon in the lattice field and the emission of a photon in the probe beam (or *vice versa*). The transition operator[14] is nearly proportional to $\mathbf{E}_{\mathrm{P}}^{(-)}(\mathbf{r}) \cdot \mathbf{E}_{\mathrm{L}}^{(+)}(\mathbf{r})$ where $\mathbf{E}_{\mathrm{L}}^{(+)}(\mathbf{r})$ is the positive frequency component of the lattice field and $\mathbf{E}_{\mathrm{P}}^{(-)}(\mathbf{r})$ is the negative frequency component of the probe field. Using

$$\begin{aligned}
\mathbf{E}_{\mathrm{L}}^{(+)}(\mathbf{r}) &= E_{+}(\mathbf{r})\,\mathbf{e}_{+} + E_{-}(\mathbf{r})\,\mathbf{e}_{-} + E_{\pi}(\mathbf{r})\,\mathbf{e}_{z} \\
\mathbf{E}_{\mathrm{P}}^{\mathrm{lg}(-)}(\mathbf{r}) &= E_{\mathrm{p}} \exp(-ik_{\mathrm{p}} z)\,\mathbf{e}_{x} \\
\mathbf{E}_{\mathrm{P}}^{\mathrm{tr}(-)}(\mathbf{r}) &= E_{\mathrm{p}} \exp(-ik_{\mathrm{p}} x)\,\mathbf{e}_{z}
\end{aligned}$$

where $\mathbf{E}_{\mathrm{P}}^{\mathrm{lg}(-)}(\mathbf{r})$ stands for the longitudinal probe and $\mathbf{E}_{\mathrm{P}}^{\mathrm{tr}(-)}(\mathbf{r})$ for the transverse probe; k_{p} is the modulus of the probe wavevector, which is essentially equal to that of the lattice beams k.

Using an expansion up to second order in x, y, z of $\mathbf{E}_{\mathrm{L}}^{(+)}(\mathbf{r})$ and $\mathbf{E}_{\mathrm{P}}^{(-)}(\mathbf{r})$ near $\mathbf{r} = 0$ (corresponding to a π-polarized site), one finds that

$$\mathbf{E}_{\mathrm{L}}^{(+)}(\mathbf{r}) \cdot \mathbf{E}_{\mathrm{P}}^{\mathrm{lg}(-)}(\mathbf{r}) \propto -ik_s x + k_s x z\,(k_c - k_{\mathrm{p}})$$

and that

$$\mathbf{E}_{\mathrm{L}}^{(+)}(\mathbf{r}) \cdot \mathbf{E}_{\mathrm{P}}^{\mathrm{tr}(-)}(\mathbf{r}) \propto 2 - ik_{\mathrm{p}} x - k_s^2 \frac{x^2 + y^2}{2} - k_c^2 z^2 - k_{\mathrm{p}}^2 x^2$$

Thus for both probes the expansion of the scalar operator $\mathbf{E}_{\mathrm{P}}^{(-)}(\mathbf{r}) \cdot \mathbf{E}_{\mathrm{L}}^{(+)}(\mathbf{r})$ does not contain any term linear in z near the bottom of a potential well. The only linear terms correspond to a transverse motion (in the $x\mathrm{O}y$ plane).

References

1. See for example P.S. Jessen, I.H. Deutsch in *Advances in Atomic, Molecular, and Optical Physics* **37**, edited by B. Bederson and H. Walther (Academic Press, Cambridge, 1996), p. 95; G. Grynberg, C. Triché in *Proceedings of the International School of Physics Enrico Fermi, Course CXXXI 1996*, edited by A. Aspect, W. Barletta and R. Bonifacio (IOS Press, Amsterdam) p. 243; A. Hemmerich, M. Weidemüller, T. W. Hänsch, *ibid.*, p. 503.
2. J.-Y. Courtois, S. Guibal, D.R. Meacher, P. Verkerk, G. Grynberg, Phys. Rev. Lett. **77**, 40 (1996).
3. T.W. Hodapp, C. Gerz, C. Furthlehner, C.I. Westbrook, W.D. Phillips, J. Dalibard, Appl. Phys. **B60**, 135 (1995).
4. C. Jurczak, B. Desruelle, K. Sengstock, J.-Y. Courtois, C.I. Westbrook, A. Aspect, Phys. Rev. Lett. **77**, 1727 (1996).
5. P. Verkerk, B. Lounis, C. Salomon, C. Cohen-Tannoudji, J.-Y. Courtois, G. Grynberg, Phys. Rev. Lett. **68**, 3861 (1992); P.S. Jessen, C. Gerz, P. Lett, W.D. Phillips, S.L. Rolston, R. Spreeuw, C.I. Westbrook, Phys. Rev. Lett. **69**, 49 (1992).
6. A. Hemmerich, T.W. Hänsch, Phys. Rev. Lett. **70**, 410 (1993); G. Grynberg, B. Lounis, P. Verkerk, J.-Y. Courtois, C. Salomon, Phys. Rev. Lett. **70**, 2249 (1993); A. Hemmerich, C. Zimmermann, T.W. Hänsch, Europhys. Lett. **22**, 89 (1993).
7. A. Kastberg, W.D. Phillips, S.L. Rolston, R.J.C. Spreeuw, P.S. Jessen, Phys. Rev. Lett. **74**, 1542 (1995).
8. J. Dalibard, C. Cohen-Tannoudji, J. Opt. Soc. Am. **B6**, 2023 (1989); P.J. Ungar, D.S. Weiss, E. Riis, S. Chu, J. Opt. Soc. Am. **B6**, 2058 (1989).
9. Y. Castin, J. Dalibard, Europhys. Lett. **14**, 761 (1991).
10. J.-Y. Courtois, G. Grynberg, Phys. Rev. A **46**, 7060 (1992).
11. C. Mennerat-Robilliard, L. Guidoni, J.-Y. Courtois, G. Grynberg, Europhys. Lett. **38**, 429 (1997).
12. K.I. Petsas, A.B. Coates, G. Grynberg, Phys. Rev. A **50**, 5173 (1994).
13. P. Verkerk, D.R. Meacher, A.B. Coates, J.-Y. Courtois, S. Guibal, B. Lounis, C. Salomon, G. Grynberg, Europhys. Lett. **26**, 171 (1994).
14. D.R. Meacher, S. Guibal, C. Mennerat, J.-Y. Courtois, K.I. Petsas, G. Grynberg, Phys. Rev. Lett. **74**, 1958 (1995).
15. C. Triché, D. Boiron, S. Guibal, D.R. Meacher, P. Verkerk, G. Grynberg, Opt. Commun. **126**, 49 (1996); K.I. Petsas, J.-Y. Courtois, G. Grynberg, Phys. Rev. A **53**, 2533 (1996).
16. M. Gatzke, G. Birkl, P.S. Jessen, A. Kastberg, S.L. Rolston, W.D. Phillips, Phys. Rev. A **55**, R3987 (1997).
17. C. Cohen-Tannoudji, in *Fundamental Systems in Quantum Optics*, Proceedings of the Les Houches Summer School of Theoretical Physics, Les Houches, 1990, Session LIII, edited by J. Dalibard, J.-M. Raimond and J. Zinn-Justin (Elsevier Science, Amsterdam, 1992).
18. B. Lounis, J.-Y. Courtois, P. Verkerk, C. Salomon, G. Grynberg, Phys. Rev. Lett. **69**, 3029 (1992).
19. S.-Q. Shang, B. Sheehy, H. Metcalf, P. van der Straaten, G. Nienhuis, Phys. Rev. Lett. **67**, 1094 (1991).
20. J.-Y. Courtois, Ann. Phys. (Paris) **21**, pp. 1-265 (1996).
21. M. Kozuma, K. Nakagawa, W. Jhe, M. Ohtsu, Phys. Rev. Lett. **76**, 2428 (1996).
22. L. Guidoni, C. Triché, P. Verkerk, G. Grynberg, Phys. Rev. Lett. **79**, 3363 (1997).

[14] We only consider here the scalar part of the operator.